Pengcheng Zhao, Qun Wang, Peihua Wang, Shenglan Xiao, Yuguo Li. (2021).

Influence of network structure on contaminant spreading efficiency**.** *Journal of Hazardous Materials***.**

doi: 10.1016/j.jhazmat.2021.127511

Influence of network structure on contaminant spreading efficiency

Pengcheng Zhao

Qun Wang

Peihua Wang

Shenglan Xiao

Yuguo Li

Department of Mechanical Engineering, The University of Hong Kong, Pokfulam, Hong Kong SAR, China

School of Public Health (Shenzhen), Sun Yat-sen University, Shenzhen, China

School of Public Health, The University of Hong Kong, Pokfulam, Hong Kong SAR, China

Corresponding author: Yuguo Li, Department of Mechanical Engineering, The University of Hong Kong, Pokfulam, Hong Kong SAR, China; School of Public Health, The University of Hong Kong, Pokfulam, Hong Kong SAR, China

Email: liyg@hku.hk

Address: 7/F, Haking Wong Building, Pokfulam, Hong Kong SAR

Submitted to *Journal of Hazardous Materials* Aug 24 2021
Accepted October 2021

Author Biographies

Pengcheng Zhao, PhD, is an Associate Professor in the School of Energy and Environment at Southeast University, China. His research centers on the built environment, with active projects involving the modeling and experimental investigation of human behavior, indoor microbial transmission, and mechanisms of infection spread.

Qun Wang, PhD, is an Assistant Professor in the Department of Environmental Science and Engineering, Macau University of Science and Technology. His research interests include high-resolution urban thermal environments, climate-change impacts on urban systems and air quality.

Peihua, PhD, Postdoctoral Research Scientist in the Department of Epidemiology, Mailman School of Public Health, Columbia University. His research interest sits at the interface of infectious disease modeling and building environmental engineering. His current research topics include spatial infectious disease epidemiology, climate epidemiology, built environment, and environmental microbiome.

Shenglan Xiao, PhD, is an associate professor at the School of Public Health (Shenzhen) in Sun Yat-sen University. Her research interests are at the intersection of public health and the built environment. Her current research focuses on the role of indoor environmental quality in the transmission of infectious diseases.

Yuguo Li, PhD, is Chair Professor of Building Environment, Honorary Professor of School of Public Health, Associate Dean (Research) of Engineering. His research interests are in building environment engineering. His current research topics include city climate/environment, environment studies of infection and indoor environment.

Influence of network structure on contaminant spreading efficiency

Abstract

Contaminants, such as pathogens or non-living substances, can spread through the interaction of their carriers (e.g., air and surfaces), which constitute a network. The structure of such networks plays an important role in the contaminant spread.

We measured the contaminant spreading efficiency in different networks using a newly defined parameter. We analyzed basic networks to identify the effect of the network structure on the contaminant spread. The spreading efficiency was highly related to some network parameters, such as the source node's average path length and degree, and considerably varied with the transfer rate per inter-node interaction. We compared the contaminant spreading efficiencies in some complex networks, namely scale-free, random, regular-lattice, and bipartite networks, with centralized, linear, and fractal networks. The contaminant spreading was particularly efficient in the fractal network when the transfer rate was ~0.5.

Two categories of experiments were performed to validate the effect of the network structure on contaminant spreading in practical cases: (I) gas diffusion in multi-compartment cabins (II) bacteria transfer in multi-finger networks. The gas diffusion could be well estimated based on the diffusion between two compartments, and it was considerably affected by the network structure. Meanwhile, the bacteria spread was generally less efficient than expected.

(200 words)

Keywords: Entropy, Fomite transmission, Fractal network, Staphylococcus aureus, Sulfur hexafluoride

1 Introduction

The study of different contaminants often involves their spread in networks of variable scales, such as the diffusion of pathogen-laden aerosol particles in multiroom areas [1], the transfer of chemical residues among environmental surfaces [2], and the spread of contaminants in a water-distribution system [3]. An individual, inanimate surface, or room of air can be considered a node that provides or receives contaminants. The interaction between any two nodes that causes contaminant transfer/exchange is considered to form an edge, such as aerosol particle deposition from air to ground, pathogen transfer when a hand touches a fomite surface, and heat transfer between rooms [4-6]. The presence of one or multiple types of nodes together with the edges makes up a spreading network.

Pathogens are a type of contaminant that can hide in inanimate carriers that are in the same network with susceptible individuals, presenting a higher infection risk [7-9]. For instance, handwashing can reduce infection risk [10, 11]. However, pathogens can also hide on surroundings and be transferred to the washed hands or food as touching actions continue [12, 13]. Moreover, pathogen-laden aerosols can remain alive in heating, ventilation, and air conditioning systems and be released into indoor air when the system restarts [1, 14]. Thus, periodic handwashing or indoor cleaning only eliminates a part of pathogens within a network, but the infection risk remains [15, 16].

Spreading networks have been modeled using various mathematical graphs, such as scale-free, random, and bipartite networks [17, 18]. As inter-node interactions proceed in a network, the number of contaminated carriers usually increases following a logistic or logarithmic growth curve [19, 20]. However, the spreading efficiency varies among networks and strongly

depends on the network structure, even among networks with the same values of relevant parameters (e.g., average path length and clustering coefficient) [21-23]. For instance, contaminants show a higher spreading efficiency in scale-free networks than in regular lattices [24]. Considering the limited effects of handwashing and indoor air purification, we aim to reduce the contamination risk by optimizing the network structure. However, without a systematic study, identifying the network structures with a high contamination risk is difficult.

Unlike the dissemination of information, which is duplicated as it spreads, contaminants can be continuously released by a source but cannot be duplicated while spreading in a network [25]. In this study, we use the evenness of the contaminant distribution at different moments in a network to quantify the contaminant spreading efficiency. We present different basic networks and propose a new parameter E as a measure to compare their contaminant spreading efficiencies under different spreading paths, transfer rates per inter-node interaction, and rounds of interactions. We also compare the spreading efficiencies in some common complex networks, including scale-free, random, regular-lattice, and bipartite networks. Furthermore, the effect of the network structure on practical spreading cases is validated through two categories of experiments. In experiment I, sulfur hexafluoride (SF_6) was used as a tracer gas to be diffused in multi-compartment cabins. In experiment II, *Staphylococcus aureus* was used as a model strain to be transferred in multi-finger networks. Overall, we illustrate the effect of the network structure on contaminant spreading and present a new perspective on the prevention of contaminant spreading.

2 Materials and method

2.1 A new parameter *E*

2.1.1 Definition of a network

To investigate contaminant spreading among multiple carriers, we modeled the spreading process using a time-series network. The carriers were considered the network nodes, and a

connection of a pair of nodes between which contaminant transfer/exchange occurs was considered an edge that preserves time-series information [26].

To generate a network with N nodes and M sequenced edges ($M \geq N-1$), we first assigned node 1 as the node of the contamination source and connected node 2 to node 1 to form edge 1. Then, we extended the network by connecting a new node to a random node in the existing network framework each time to form a new edge. After all of the N nodes were connected, we obtained a basic network with $N-1$ edges ($N-1$ is the least number of edges to form an N-node network). For a complex network with extra edges (when $M > N-1$), the extra $M-N+1$ edges were added one-by-one by randomly connecting two nodes at a time. Thus, the contaminant spread was completely defined by the network, in which the edges and their sequence denoted the inter-node interactions and the interacting sequence, respectively.

The network structure likely varied, as each added node could connect different existing nodes, and the formed edges had a sequence. In this study, a "network structure" refers to

I. the source position (i.e., the node that is initially contaminated to serve as the contaminant source);

II. the framework (i.e., the pairs of nodes interacting as edges); and

III. the edge sequence (i.e., the time series of inter-node interactions).

In network generation, the existing nodes have different probabilities of connecting with the newly added node (or another existing node) to form a new edge, and the probability distribution determines the network type. For instance, if the probability of an existing node being connected is proportional to the degree of the existing node, the generated network is a scale-free network.

2.1.2 Contaminant spread in a network

For a pair of interacting nodes, contaminants can be transferred from one node (the contaminant donor) to another (the recipient) at a certain rate [27]. The transfer rate τ_{DR} can be

obtained using Equation 1a, in which C_D and C_R are the contaminant contents on the donor and recipient after an interaction, respectively, and C is the original contaminant content on the donor before the interaction, such that $C = C_D + C_R$.

For any two nodes that have both been contaminated, we calculate the contaminant exchange in the interaction by iterating the numbers of contaminant particles on the nodes considering both transfer directions, as in Equation 1b. The variation of contaminant contents on the two nodes thus depends on the net transfer amount. If the nodes are homogeneous (i.e., they have similar contaminant retention abilities), the transfer rates in the two directions are equal; that is, $\tau_{DR} = \tau_{RD}$ [28].

Furthermore, we calculate the contaminant spread in a network with N nodes. We define an interaction round as all of the inter-node interactions performed following the edge sequence. To calculate the contaminant spread in an interaction round, we iterate the contaminant contents on all of the N nodes (C_1, C_2, …, C_N) following the inter-node interaction sequence (Equation 1c) and obtain the contaminant distribution on the nodes. Equation 1c also includes a flow rate (R_{Flow}) and a decay rate (R_{Decay}) to simulate the continuous release of contaminant by the source node and the contaminant decay in a network.

$$\tau_{DR} = \frac{C_R}{C} = \frac{C_R}{C_D + C_R} \tag{1a}$$

$$\Rightarrow \quad [C_D \quad C_R] = [C_D \quad C_R] \times \begin{bmatrix} 1-\tau_{DR} & \tau_{DR} \\ \tau_{RD} & 1-\tau_{RD} \end{bmatrix} \tag{1b}$$

$$\Rightarrow \quad \begin{bmatrix} C_1 \\ C_2 \\ \vdots \\ C_N \end{bmatrix}^T = \begin{bmatrix} C_1 \\ C_2 \\ \vdots \\ C_N \end{bmatrix}^T \times \prod_{i \neq j} \begin{bmatrix} 1 & & & \\ & 1-\tau_{ij} & & \tau_{ij} \\ & & 1 & \\ & \tau_{ji} & & 1-\tau_{ji} \\ & & & & 1 \end{bmatrix} \times (1 - R_{Decay}) + \begin{bmatrix} R_{Flow}C \\ 0 \\ \vdots \\ 0 \end{bmatrix}^T \tag{1c}$$

where the combination of i and j represents all of the pairs of interacting nodes in an interaction round, $R_{Flow} \times C$ denotes the release of contaminant on the source node after each interaction round, and R_{Decay} denotes the decay rate of the contaminant on each node per interaction round.

In an ideal situation, the contaminant concentration approaches a uniform value after

sufficient interaction between two homogeneous nodes [28]. Thus, if the two nodes have the same size, the contaminant content on them will be identical, indicating a transfer rate of τ = 0.5; otherwise, the transfer rate at uniform concentration should be calculated using Equation 2.

The size of a node (A) can be specified as the volume for room nodes or area for surface nodes. To calculate the contaminant transfer rate between nodes of different sizes, we assume that after an interaction between a contaminated node (donor) and a clean node (recipient), the ratio of the resultant contaminant concentrations of the two nodes is independent of node size [28]. Thus, we define the distribution ratio (β_{DR}) as the ratio of the contaminant concentration on the donor and recipient nodes after an interaction (Equation 2a). We can obtain the distribution ratio β_{DR} from the measured transfer rate between two same-size nodes (τ) (Equation 2b), and the transfer rate between any pair of nodes (τ_{DR}) can be accordingly derived (Equation 2c).

$$\beta_{DR} = \frac{C_D/A_D}{C_R/A_R} = \frac{A_R(1-\tau_{DR})}{A_D\tau_{DR}} \tag{2a}$$

$$\beta_{DR} = \frac{1-\tau}{\tau} \quad \text{, when } A_D = A_R \tag{2b}$$

$$\Rightarrow \quad \tau_{DR} = \left(\frac{A_D}{A_R}\beta_{DR} + 1\right)^{-1} = \left[\frac{A_D(1-\tau)}{A_R\tau} + 1\right]^{-1} \tag{2c}$$

where A_D and A_R represent the donor and recipient node sizes, respectively.

2.1.3 The evenness of contaminant distribution in a network

The parameter E, a function of the entropy of contaminant distribution, is proposed to quantify the evenness of the contaminant distribution in a network [29]. The contaminant concentration on node i, a subregion in an N-node network, is $P_i = C_i/A_i$, assuming uniform contaminant distribution on the node. The probability that a randomly selected particle is from a given unit size at node i can be calculated as $p_i = C_i/(A_i \times \sum_{i=1}^{N} C_i)$. Thus, the information

required to find this particle is its Shannon entropy, defined as $H_i = \sum_{i=1}^{N}[A_i \times (-p_i \ln p_i)]$; moreover, the information required to locate all of such particles (H) can be calculated using Equation 3a [29], and H reaches its maximum (i.e., H_{max}) when the contaminant particles in the network are evenly distributed. The entropy difference (ΔH) between the current particle distribution and an even distribution can be calculated using Equation 3b. To better visualize the contaminant distribution evenness in a plot, we propose the parameter E (Equation 3c), as an exponential function of ΔH. Details of the derivation are provided in Appendix A.3.

$$\begin{cases} H = C \times \sum_{i=1}^{N}[A_i \times (-p_i \ln p_i)] \quad \text{where}, p_i = \dfrac{C_i}{A_i \sum_{j=1}^{N} C_j} \\ H_{max} = C \times \sum_{i=1}^{N}[A_i \times (-p_{even} \ln p_{even})] \quad \text{where}, p_{even} = \dfrac{1}{\sum_{j=1}^{N} A_j} \end{cases} \tag{3a}$$

$$\Delta H = H - H_{max} = \sum_{i=1}^{N}\left[C_i \times \ln\left(\frac{A_i / \sum_{j=1}^{N} A_j}{C_i / \sum_{j=1}^{N} C_j}\right)\right] \tag{3b}$$

$$E = \exp(N \times \Delta H) = \prod_{i=1}^{N}\left[\left(\frac{A_i / \sum_{j=1}^{N} A_j}{C_i / \sum_{j=1}^{N} C_j}\right)^{N \times C_i}\right] \tag{3c}$$

In this study, we mainly focus on contaminant evenness in a network. We assume that the contaminant content in a network is constant ($\sum_{j=1}^{N} C_j = C$) and that the initial content on the node of the contaminant source is $C = 1$. The parameter E can be also interpreted from another perspective. As each contaminant particle on node i possesses a size (e.g., area/space) of A_i/C_i on average, E equals the weighted geometric mean of the size occupied by each contaminant particle throughout the N nodes (after non-dimensionalization). E is varied between 0 and 1. A larger E indicates a more even distribution of contaminants in a network, and E reaches its maximum (= 1) under a perfectly even distribution. In Equation 3c, a power of N is introduced, which amplifies the difference in E values between networks. However, it is still debatable whether it is appropriate to use the current E with a power of N, i.e., $E = \exp(N \times \Delta H)$ as in Equation 3c, instead of defining it as $E = \exp(\Delta H)$.

2.2 Quantifying contaminant spreading efficiency in networks by their *E* values

First, we compared the contaminant spreading efficiencies in different networks by comparing their *E* values under different conditions. Two groups of networks were considered:

I. Basic networks: $N \leq 8$.

II. Complex networks, at $\tau = 0.5$.

To focus on the effect of network structure on contaminant spreading efficiency while eliminating the effect of external factors, the networks were set with same-size homogeneous nodes, unweighted and non-directional edges, and a constant contaminant transfer rate through inter-node interactions.

Then, we performed two categories of laboratory experiments to validate the influence of network structure on contaminant spreading in practical cases.

III. SF_6 was used as a tracer gas to measure the gas diffusion in multi-compartment cabins.

IV. *S. aureus* was used as a model strain to investigate bacteria spread in multi-finger networks.

In each experiment, the target contaminants (i.e., SF_6 or *S. aureus*) were spread among their carriers (i.e., compartments or fingers with varying sizes) as the nodes interacted, according to the structures of networks VII–X in Figure 1. The air temperature in the laboratory was maintained at 24 ± 1°C, with a relative humidity of 60%−70%. Permission was obtained from the Human Research Ethics Committee of The University of Hong Kong (ethical approval code: EA1603004).

2.2.1 Contaminant spread in basic networks

In this study, we used MATLAB programs to generate the networks with *N* homogeneous nodes ($N \leq 8$) and $N - 1$ nondirectional edges, without tadpoles or double links in the structure. Each node in a network was connected to at least one other node, forming an edge, and the

edges were numbered from 1 to $N-1$ to define the sequence of the inter-node interactions. For each basic network in this study, E was calculated under varying contaminant transfer rates (τ = 0.1, 0.3, 0.5, 0.7, and 0.9), flow rates per interaction round (R_{Flow} = 0 and 0.2), and interaction rounds (T = 1–10). The MATLAB programs and the data are in Appendix B.

There were 0, 1, 2, 5, 14, 42, 132, and 429 networks as N increased from 1 to 8. For each network, two parameters for the source node were calculated: the average path length (L), that is, the average path length to the other $N-1$ nodes (there is only one path for each pair of nodes in the basic networks), and the degree (D), that is, the number of edges attached to the source node.

<Figure 1>

(Shown in a single-column fitting image)

2.2.2 Contaminant spread in complex networks

We analyzed the differences in contaminant spreading efficiencies between some complex networks that frequently occur in real situations. We used MATLAB to randomly generate 20 networks for each of the scale-free (generated referring to the BA model [30]), random (generated referring to the ER model [31]), regular-lattice (8 × 8 nodes), and bipartite (26 nodes vs. 38 nodes) networks, with each network having 64 nodes and 112 edges. The networks are defined in Appendix A.5, where the method to automatically generate the networks is introduced. For comparison, we also analyzed three typical networks, namely fractal, centralized, and linear networks, with each having 64 nodes and 63 edges. In summary, there were 83 networks. The MATLAB codes and the adjacency matrixes of the generated networks are attached in Appendix B. For each network, E was calculated for a transfer rate of τ = 0.5 after different interaction rounds (T = 1–12), and the spreading efficiencies of the networks

were compared accordingly.

2.2.3 Gas diffusion in multi-compartment cabins

We used SF_6 as a tracer gas for diffusion in a multi-compartment cabin. We used acrylic boards to assemble a transparent cabin with total inner dimensions of 1,200 (l) × 800 (w) × 300 (h) mm^3 (see Figure A8 in Appendix A.6). The cabin was divided by pluggable acrylic boards into five compartments with different dimensions, that is, five nodes of different sizes: a large compartment (400 × 800 × 300 mm^3) as the SF_6 source and four small compartments (400 × 400 × 300 mm^3). Each pluggable acrylic board had a door of 100 (w) × 200 (h) mm^2. We used thin threads and a magnet pair to control the opening and closing of each door. The doors connecting the five compartments were taken as the time-series edges. The layouts of the five compartments with four doors are shown in Figure 2; four networks were assembled following the structures of networks VII–X in Figure 1. Five polyvinyl chloride tubes connected to air channels 1–5 in a gas multipoint sampler (INNOVA 1409, LumaSense Technologies, Ballerup, Denmark) were inserted into the five compartments to sample SF_6. A photoacoustic gas monitor (INNOVA 1412i, LumaSense Technologies, Ballerup, Denmark) was connected to the sampler to measure the SF_6 concentration [32]. The monitor could only measure one channel from the sampler at a time. Once SF_6 started diffusing in the cabin, the monitor continuously measured the SF_6 concentrations channel-by-channel.

During the test of each network, we first injected approximately 200 ml of SF_6 into the source compartment using a mass flow controller. We opened and closed the doors according to the corresponding edge sequence in Figure 1 to diffuse SF_6 between any pair of compartments (i.e., to exchange air in the two rooms). Each door was opened at 90° for 6–8 min and then closed immediately before the next door was opened. After the four doors were opened and closed once, a round of gas diffusion was complete, and the last measured SF_6 concentrations in the five compartments were used to calculate E using Equation 3c. For each

network, we continuously performed eight diffusion rounds ($T = 8$). Details of the SF_6 diffusion tests are presented in Appendix A.6.

<Figure 2>

(Shown in a single-column fitting image)

2.2.4 Bacterial spread in multi-finger networks

The bacteria spread was investigated in four multi-finger networks designed following the structures of networks VII–X in Figure 1. For the test of each network, we assigned a specific finger pad for each node (Table 1). Thus, five fingers with different areas were used as five nodes with different sizes. Before experiment, lysogeny broth (LB) and 1.5% LB agar were prepared for the bacteria incubation and plate counting, respectively. Hands used for finger touches were repeatedly washed following WHO guidelines for handwashing [33], sprayed with 75% ethanol, and air-dried. The washed hands did not touch any surface before the experiment.

We spread bacteria by performing finger–finger touches. We measured the touching area of each finger pad according to the method introduced by Dzidek et al. [34]. The nominal contact area in a touch was approximately 4.6 cm^2 for a thumb pad and 2.8 cm^2 for the index, middle, and ring finger pads. To perform a finger–finger touch, a three-step touching pattern was performed (indicated by arrows 1, 2, and 3 in Figure 3). The two fingers tightly touched each other for 10 s and then separated; during the touch, the two finger pads rubbed each other 10 times in a twisting 90° back-and-forth movement.

During the test of each network, a 20 μL *S. aureus* (ATCC 25923) suspension was first inoculated on the finger pad of the contaminant source with an area of approximately 1 cm^2 (*S. aureus* would spread to the entire touched area of each finger pad in the subsequent touches),

and air-dried to visible dryness, which required approximately 20 min. Then, fingers were touched following the network structure defined in Figure 1. Different numbers of touch rounds (T = 1, 2, 4, and 8) were repeated for each network. The proportions of *S. aureus* on fingers after the different numbers of touch rounds were evaluated, and the average proportions obtained from three replicates were used to calculate E following Equation 3c. For the *S. aureus* quantification, each bacteria-contaminated finger pad was sampled through a sequential sampling method [35, 36]. The specific process for quantifying the finger bacteria is introduced in Appendix A.7.

<Figure 3>

(Shown in a single-column fitting image)

<Table 1>

The E value of contaminant distribution in a network can be used to reversely estimate the contaminant transfer rate per inter-node interaction (τ) and flow rate per interaction round (R_{Flow}).

For a network, we can obtain the contaminant distribution through experiments and then calculate the corresponding "experimental E" value; the contaminant distribution can also be predicted using Equation 1c and different values of τ and R_{Flow}, after which a series of "predicted E" values can be calculated, each corresponding to a pair of τ and R_{Flow}. Of all of the combinations of τ and R_{Flow}, the pair whose corresponding predicted E generated the smallest difference with the experimental E is the best estimate of τ and R_{Flow}.

In this study, we performed three categories of experiments: gas diffusion (Section 2.2.3),

bacteria spread (Section 2.2.4), and a test of gas diffusion at a flow rate R_{Flow} of 0.2–0.25 (Appendix A.8). For each category, we calculated the experimental E values based on the experimental results and then obtained our best estimates of τ and R_{Flow}. We also compared the estimated τ and R_{Flow} with the τ and R_{Flow} from an independent measurement to validate the effectiveness of this estimation method. The results are presented in Appendix A.8.

3 Results

3.1 Contaminant spread in basic networks

The contaminant spreading efficiencies among different basic networks were compared. Figure 4 illustrates the E values for different networks with varying numbers of nodes (N), transfer rates per interaction (τ), interaction rounds (T), flow rates per interaction round (R_{Flow}), and average path lengths of the source node (L). Similar to the nature of entropy, the value of parameter E in a network increases irreversibly as the inter-node interactions proceed. Here, a higher number of interaction rounds (larger T) resulted in a more even contaminant distribution. However, the relationships between some parameters and E varied with the transfer rate (Table 2).

As shown in Figure 4a, E was larger on average when N was smaller, indicating that contaminant spreading efficiency was higher for the networks with fewer nodes, owing to their shorter average path lengths. Contaminants in the networks of identical frameworks (same colors in each plot in Figure 4) can have different spreading paths, resulting in different E values. For example, networks I, II, and III (Figure 1, also marked in Figure 4a) had an identical framework, and the source nodes in networks II and III were in the same position. However, their spreading efficiencies varied considerably because of their different edge sequences (see the second plot of the first row in Figure 4a).

A network exhibited various spreading efficiencies under different transfer rates. When the transfer rate was small (e.g., $\tau = 0.1$), the networks with a centralized structure or shorter

average path length of the source node (L) showed a higher spreading efficiency (Figure 4b). When the transfer rate was large (e.g., $\tau = 0.9$), the networks with a linear structure or a larger L showed a higher spreading efficiency. Generally, the spreading efficiency was on average the highest at a transfer rate of approximately 0.5–0.7, (Figure 4b). However, very few practical cases can be found with transfer rates significantly larger than 0.5. Networks with different structural characteristics showed their maximum spreading efficiencies at varying transfer rates. A series of networks occurred only at $N = 2^x$ ($x = 1, 2, 3...$), in which contaminants were evenly distributed immediately after an interaction round ($T = 1$) when the transfer rate τ was 0.5. This series of networks had a fractal structure (Figure A7 in Appendix A.5). Networks II and VI in Figure 1 are typical fractal networks with $N = 4$ and 8, respectively.

In addition, the existence of contaminant flow decreased the contaminant spreading efficiency, because the flow continuously disturbed the equilibrium of contaminant distribution. As shown in the third and fourth columns of the plots with the same transfer rate in Figure 4b, the contaminant spreading slowed upon introducing a flow rate ($R_{Flow} = 0.2$). We also illustrate the variation of E as a function of different parameters (Figures A3–A6 in Appendix A.4).

<Figure 4>

(shown in a 2-column fitting image)

<Table 2>

3.2 Contaminant spread in complex networks

We randomly generated 20 complex networks for each of the four representative structures (scale-free, random, regular-lattice, and bipartite) (Figure 5), and their contaminant

spreading efficiencies with respect to their E values were compared after different interaction rounds (T = 1, 4, 8, and 12) with a transfer rate of τ = 0.5. Generally, the distributions of data points in the plots are similar to the patterns in the plots of τ = 0.5 in Figure 4b; however, the E values in Figure 5 increase more slowly in the larger network (N = 64). At τ = 0.5, the fractal network exhibited the largest E, whereas the E values for the centralized and linear networks were extremely small. The random networks showed relatively high spreading efficiencies. However, the efficiencies varied considerably within each type of network (random, bipartite, and scale-free), because the degree varied substantially among the nodes. In particular, a network with its contaminant source at a marginal node showed much lower spreading efficiency than that with its contaminant source at a hub node. Additionally, the spreading efficiencies of most of the regular-lattice networks were very low, unless the source node was situated close to the center of the 8 × 8 grid. In summary, as the interaction round (T) increased, the average spreading efficiencies of the different network types in Figure 5 were in the following order at $\tau \approx 0.5$: fractal > random > bipartite ≈ scale-free > regular-lattice > centralized ≈ linear, which is consistent with the results of several studies [24, 37-39]. This ranking demonstrates the relative efficiency of complex real-world networks, such as small-world networks and networks with multiple communities, as their characteristics are close to those of scale-free networks [40-42].

<Figure 5>

(Shown in a 2-column fitting image)

3.3 Gas diffusion in multi-compartment cabins

We measured the SF_6 concentration as the gas diffused in four types of multi-compartment cabins. The mass ratio in each compartment is illustrated with the columns in Figure 6a. In a

separate measurement, we diffused SF_6 between two same-size compartments (400 × 400 × 300 mm^3), with one filled with approximately 200 ml of SF_6. After 7 min, the SF_6 concentration ratio of the two same-size compartments was 0.512:0.488, indicating a transfer rate τ of 0.488. Based on this value, we predicted the SF_6 transfer rates between different compartments (τ_{DR}) using Equation 2c and consequently the SF_6 distributions in the four networks using Equation 1c, and compared them with the corresponding experimental data, as shown in Figure 6a.

A high SF_6 diffusion efficiency could be obtained under our experimental conditions, as the measured distribution ratio β_{DR} of 0.512/0.488 was close to the ideal value of 1. Predictions of SF_6 distribution based on this distribution ratio were close to the experimental results (see Figure 6a). Both the experimental data and the predicted results show that the source compartments whose size was twice that of the others maintained a higher SF_6 mass ratio.

Furthermore, we predicted the E values at varying transfer rates (τ = 0–1) and compared them with the experimental E (blue curves and cross-points in Figure 7). The E values more clearly reflected the difference between the predicted results and the experimental data, and between different networks. As shown in Figure 7, the SF_6 diffusion efficiency in the experiments could be well predicted based on a known transfer rate. The SF_6 diffusion efficiency in network VII, which had a linear structure, was lower than those in the other three networks, despite network VII having the same framework as network X (see Figure 1), demonstrating the effect of network structure on contaminant spreading efficiency.

3.4 Bacterial spread in multi-finger networks

We spread *S. aureus* in four types of multi-finger networks through finger–finger touches. The bacteria distribution in each network was evaluated after different touch rounds (T = 1, 2, 4, and 8), as shown in the columns in Figure 6b. In a separate measurement, we measured the transfer rate in an inter-index finger touch as τ = 0.403. Based on this value, we predicted the *S. aureus* transfer rates between different fingers (τ_{DR}) using Equation 2c and consequently the

S. aureus distributions in the four networks using Equation 1c, and compared them with the corresponding experimental data in Figure 6b.

After eight touch rounds, the *S. aureus* distributions in all of the networks were similar, in which the thumbs, with larger finger pad areas, held more bacteria (first two columns in each plot in Figure 6b), and the other fingers had fewer. However, different multi-finger networks exhibited different spreading process. In networks VII and X, bacteria continuously transferred from the donor finger to the other four fingers, whereas in networks VIII and IX, the first-touched finger (the second column in each plot in Figure 6b) in the first four rounds of touches (T = 1–4) harbored more bacteria than the donor finger (the first column in each plot in Figure 6b).

Although in Figure 6b, the predicted results are close to the experimental data, a comparison of the E values from the predicted results and experimental data (red curves and cross-points in Figure 7) shows that the spreading efficiency of *S. aureus* in multi-finger networks was considerably lower than expected. We reversely estimated the bacteria transfer rate using the experimental data (see Figure 8) and obtained the average transfer rate in the experiments as τ = 0.180, which was smaller than the 0.403 value obtained from a separate measurement (a single touch between two index fingers). The smaller average transfer rate of *S. aureus* spreading in the networks was likely due to the slowing down of bacteria spread among fingers as the touching proceeded. Previous research has shown that bacteria cells adhering more firmly to a recipient finger are usually harder to move to the next finger in subsequent touching actions [27].

<Figure 6>

(Shown in a 1.5-column fitting image)

<Figure 7>

(Shown in a 1.5-column fitting image)

3.5 Estimating the transfer rate according to the experimental *E* value

The estimated τ and R_{Flow} for different spreading processes are shown in Figure 8. During SF_6 diffusion without a flow rate (experiments in Section 2.2.3), the estimation of the transfer rate τ was accurate, as the estimated τ and measured τ were 0.494 and 0.488, respectively.

In *S. aureus* spread (experiments in Section 2.2.4), the estimated τ was 0.180, which was lower than the value from a separate measurement (0.403). This difference was likely due to the decrease in bacterial transfer rate during bacteria spread among fingers; this is because during touching actions, bacterial cells were continuously transferred to the finger of larger adhesion force, and it was thus harder for the bacteria to move to the next finger [27].

When we introduced a flow rate of R_{Flow} = 0.2–0.25 into the SF_6 diffusion in network VII (see Appendix A.8), the most likely τ and R_{Flow} in the gas diffusion experiment were estimated as 0.547 and 0.260, respectively, which were close to the two values from a separate experiment in which the τ between two same-size compartments was measured as 0.488.

Figure 2 Standard deviation between experimental *E* and predicted *E* under different transfer rates (τ) per inter-node interaction and flow rates (R_{Flow}) per interaction round.

Parula surface: experiment of gas diffusion in a multi-compartment cabin with gas flow; blue curve: experiment of gas diffusion in multi-compartment cabins; red curve: experiment of bacterial spread in multi-finger networks.

The orange, blue, and red asterisks in the horizontal plane represent the transfer rate and flow rate corresponding to the smallest standard deviation on the parula surface, blue curve, and red

curve, respectively.

(Shown in a single-column fitting image)

4 Discussion

In this study, we propose a new parameter E, which provides a straightforward way to illustrate contaminant distribution evenness in a network and can be applied to quantify the contaminant spreading efficiency. We observed the influences of different factors on the E value for both basic and complex networks and found that the spreading efficiency was highly related to the network structure. We performed two categories of laboratory experiments (SF_6 diffusion in multi-compartment cabins and *S. aureus* spread in multi-finger networks) to validate the effect of the network structure on practical spreading cases and demonstrated the feasibility of using the per-interaction transfer rate value (obtained from a separate measurement) to predict the contaminant spread in a network. Furthermore, we could use the E calculated from the experimental results to reversely correct the contaminant transfer rate (τ) and flow rate (R_{Flow}).

4.1 Major network-related factors influencing contaminant spreading efficiency

The variation of the E value at $N > 8$ was similar to the results at $N \leq 8$ (Figure 4). When the edge number in an N-nodes network was greater than $N - 1$, the closed-loop structures existed in the network, resulting in a higher contaminant spreading efficiency for each interaction round. Edges can also have different weights (e.g., interacting frequencies or efficiencies), which represent the heterogeneous interactions between nodes [43]. Only unweighted time-series networks were tested here.

We applied the new parameter E to some well-known complex networks. Among the networks, the fractal network showed an extremely high spreading efficiency at $\tau \approx 0.5$. Similar structures occur in living objects, such as lungs [44, 45], neural systems [46], and trees [47]. The structures of these objects evolved to become fractal-like to improve the spreading

efficiencies of oxygen, signals, and nutrition, respectively. This confirms our conclusion: the fractal network had the highest E value at an ideal transfer rate ($\tau \approx 0.5$). However, we only considered the occurrence of a single node–node interaction per time (fractal dimension $d = 2$), without considering the cases in which a source node simultaneously interacts with multiple nodes (d = 3, 4, ...). If we expand the definition of "fractal structure," more fractal networks are possible, with the highest spreading efficiency occurring at a transfer rate τ of $1/d$. For example, the centralized network with N nodes can be modified to an N-dimensional fractal network by using the source node to simultaneously interact with the other $N - 1$ nodes, and its highest spreading efficiency occurs at $\tau = 1/N$.

According to the results in Figures 4 and 5, at any transfer rate, the E values for the networks were either between those of the linear and the centralized networks under the same number of nodes or, more commonly, higher than both values. Surprisingly, the efficiency of the linear network under a high transfer rate was similar to that of the centralized network under a low transfer rate. A connection existed between the two network types. The network structure depends on how we define the nodes and contaminants. For example, a virus-laden bicycle shared by several individuals can be considered as a hub, and the viruses as the target contaminants spread indirectly between people through this hub bicycle, forming a centralized network. We can also consider the "bicycle + viruses" as a target contaminant, and the virus-laden bicycle is transferred directly from one individual to the next, forming a linear network. The transfer rate depends on the definition of "contaminant" and the network structure. However, the E value remains constant regardless of how we define the network.

4.2 Effect of network structure in real spreading cases

The effect of network structure on the *S. aureus* spreading efficiency in surface networks was not as pronounced as that on the SF_6 spreading efficiency in space networks. In this study, the spread of SF_6 between nodes occurred purely by natural diffusion without an additional

driving source, but SF_6 showed a high spreading efficiency. In the experiment, any leakage between compartments or external disturbances could further accelerate the SF_6 spread. In contrast, the *S. aureus* spreading efficiency was low. Considering that we performed repeated rubbing in each finger–finger touch, we believe that the *S. aureus* spreading efficiency had reached its maximum. Gas diffusion can therefore more easily reach an ideal even distribution than microbial spread on surfaces.

As shown in the blue scatters in Figure 7, the SF_6 diffusion efficiency in the linear network (network VII) was considerably lower than those in other networks, indicating a considerable effect of the network structure. In contrast, the *S. aureus* transfer rate gradually decreased as the touching proceeded. After the transfer of a contaminant particle from a donor surface to a recipient surface, the particle may (I) receive greater adhesive force and (II) sit deeper at the recipient than it did at the donor, which indicates a smaller transfer probability in the subsequent surface contacts [27]. Such a decrease in microbial transfer rate occurred in both this study and previous experiments [20, 36]. Owing to this phenomenon, the contaminant spreading efficiency in surface networks was often lower than expected (see the red lines and scatters in Figure 7). Therefore, the influence of network structure on the surface contaminant spreading was not pronounced. The specific mechanism and its effect will be clarified in our future study.

4.3 Role of hub nodes in a network

For either the scale-free or the regular-lattice networks, their E values were quite different, which was due to the difference in the source positions. In a scale-free network, the spread begins to outbreak only after one or more hub nodes are contaminated. In contrast, random networks have higher spreading efficiencies, because the degrees of the nodes are more evenly distributed. The bipartite networks, generated as a type of conditional scale-free network, showed a spreading efficiency similar to the scale-free networks. This indicates a likely high

contaminant spreading efficiency in numerous scenarios when a hub node is contaminated, such as in aircraft cabins [48] and hospitals [49], in which pathogens spread among human hands and inanimate surfaces. In these scenarios, the hands and surfaces constitute bipartite surfaces, as there are usually no interactions between strangers or between surfaces.

By comparing scale-free and regular-lattice networks, we observed that the existence of contaminated super-hubs considerably increased contaminant spreading efficiency, consistent with the conclusions of prior studies [24, 50]. In the experiments by Wang et al. [20] on bacteria spread in an office through human touch, the spreading network approximated a conditional bipartite scale-free network. In two sets of experiments involving networks with similar densities, the bacterial spreading efficiency was considerably affected by the node degree of the bacterial source. In addition, the existence of high-touch hands or inanimate surfaces as super-hubs in a network considerably improved the spreading efficiency.

Another case without a hub node demonstrated relatively low efficiency of contaminant spread. The apartments in a residential building typically constitute a three-dimensional regular-lattice network in which pathogens (e.g., SARS-CoV-2) can spread through air, surfaces, and sewage systems [1]. In their case study, Wang et al. [32] showed that the spread of infections was mainly restricted to adjacent apartments with a higher air exchange rate (i.e., nodes connected by a higher-weight edge), partially because that the potential super-hubs, such as the air or surfaces in elevators, lobbies, and other public areas, were not participated in pathogen spread, which avoided a larger outbreak.

4.4 Potential applications of the newly proposed theory

The new parameter proposed in this study can be used to quantify contamination risk in different networks, such as hazardous chemical diffusion in water [3], pollutant diffusion and heat exchange in air [51-53], and pathogen spread through surfaces or air [54]. In subsequent studies, we will combine node characteristics to quantify (a) the entropy (or a related parameter)

of a single node, to measure its danger as a contaminant donor, and (b) the entropy of all of the neighbors of a node, to measure the potential contamination risk of this node. Furthermore, the new parameter can also function as a measurement index in other applications involving spreading activities, such as the allocation of emergency resources (e.g., medical and firefighting supplies and power restoration capacity) [55, 56], the optimization of a transport logistics system (e.g., warehouse layout and package storage) [57], and animal migration and human transportation [58].

Furthermore, we can use the known (or partially known) distribution of contaminant in a network to reproduce the spreading process, as the new parameter provides a yardstick to estimate the probability of a likely spreading path. The theory proposed in this study might be useful for tracing a contamination source, such as in source tracking during a regional disease outbreak (e.g., COVID-19). Moreover, the pathogen spreading efficiency and the index case can be reversely derived based on patient distribution. However, we do not illustrate which networks possess higher infection risks, because higher spreading efficiency is not equivalent to a higher infection ratio [59]. A susceptible individual becomes infected only after receiving pathogens in a dose exceeding the infective dose [60], which is usually caused by repeated/extended interaction with the infection source. Such interactions can be considered high-weight edges in a pathogen-spreading network [43].

5 Conclusion

We proposed a parameter E, a function of Shannon entropy, to measure the evenness of contaminant distribution in a network. Based on the E value, we clearly illustrated the difference in contaminant spreading efficiency between varying network structures. Contaminants in fractal networks showed extremely high spreading efficiency at an ideal condition; in a random or scale-free network, contaminant spreading efficiency was considerably enhanced when a hub node was contaminated. In practical cases, experiment

results of the SF_6 distribution in multi-compartment cabins was consistent to the prediction based on its diffusion rate between a pair of compartments, and the gas diffusion was demonstrated susceptible to the structure of the cabin network. In contrast, the efficiency of *S. aureus* spread in all the enumerated multi-finger networks was substantially lower than expected. Thus, the structure of surface networks showed less effect on the bacterial spread.

Database

Appendix B. DOI: 10.17632/shpzy4c53x.1

Acknowledgements

This work was supported by the General Research Fund project from Hong Kong Research Grants Council [grant numbers 17203420].

References

[1] L. Morawska, J.W. Tang, W. Bahnfleth, P.M. Bluyssen, A. Boerstra, G. Buonanno, J. Cao, S. Dancer, A. Floto, F. Franchimon, C. Haworth, J. Hogeling, C. Isaxon, J.L. Jimenez, J. Kurnitski, Y. Li, M. Loomans, G. Marks, L.C. Marr, L. Mazzarella, A.K. Melikov, S. Miller, D.K. Milton, W. Nazaroff, P.V. Nielsen, C. Noakes, J. Peccia, X. Querol, C. Sekhar, O. Seppanen, S.I. Tanabe, R. Tellier, K.W. Tham, P. Wargocki, A. Wierzbicka, M. Yao, How can airborne transmission of COVID-19 indoors be minimised?, Environment International, 142 (2020) 105832. DOI:10.1016/j.envint.2020.105832.

[2] E.A. Cohen Hubal, M.G. Nishioka, W.A. Ivancic, M. Morara, P.P. Egeghy, Comparing surface residue transfer efficiencies to hands using polar and nonpolar fluorescent tracers, Environmental Science & Technology, 42 (2007) 934-939. DOI:10.1021/es071668h.

[3] S. Masud Rana, D.L. Boccelli, Contaminant spread forecasting and confirmatory sampling location identification in a water-distribution system, Journal of Water Resources Planning and Management, 142 (2016) 04016059. DOI:10.1061/(ASCE)WR.1943-5452.0000704.

[4] M. Salathé, M. Kazandjieva, J.W. Lee, P. Levis, M.W. Feldman, J.H. Jones, A high-resolution human contact network for infectious disease transmission, Proceedings of the National Academy of Sciences, 107 (2010) 22020-22025. DOI:10.1073/pnas.1009094108.

[5] N. Johansson, S. Svensson, P. van Hees, An evaluation of two methods to predict temperatures in multi-room compartment fires, Fire Safety Journal, 77 (2015) 46-58. DOI:10.1016/j.firesaf.2015.07.006.

[6] P.Y. Chia, K.K. Coleman, Y.K. Tan, S.W.X. Ong, M. Gum, S.K. Lau, X.F. Lim, A.S. Lim, S. Sutjipto, P.H. Lee, T.T. Son, B.E. Young, D.K. Milton, G.C. Gray, S. Schuster, T. Barkham, P.P. De, S. Vasoo, M. Chan, B.S.P. Ang, B.H. Tan, Y.S. Leo, O.T. Ng, M.S.Y. Wong, K. Marimuthu, T. Singapore Novel Coronavirus Outbreak Research, Detection of air and surface contamination by SARS-CoV-2 in hospital rooms of infected patients, Nature Communications, 11 (2020) 2800. DOI:10.1038/s41467-020-16670-2.

[7] S.Y. Bin, J.Y. Heo, M.S. Song, J. Lee, E.H. Kim, S.J. Park, H.I. Kwon, S.M. Kim, Y.I. Kim, Y.J. Si, I.W. Lee, Y.H. Baek, W.S. Choi, J. Min, H.W. Jeong, Y.K. Choi, Environmental contamination and viral shedding in MERS patients during MERS-CoV outbreak in South Korea, Clinical Infectious Diseases, 62 (2016) 755-760. DOI:10.1093/cid/civ1020.

[8] H. Kanamori, W.A. Rutala, D.J. Weber, The role of patient care items as a fomite in healthcare-associated outbreaks and infection prevention, Clinical Infectious Diseases, 65 (2017) 1412-1419. DOI:10.1093/cid/cix462.

[9] S. Asadi, N. Gaaloul Ben Hnia, R.S. Barre, A.S. Wexler, W.D. Ristenpart, N.M. Bouvier, Influenza A virus is transmissible via aerosolized fomites, Nature Communications, 11 (2020) 4062. DOI:10.1038/s41467-020-17888-w.

[10] A.M. Wilson, K.A. Reynolds, R.A. Canales, Estimating the effect of hand hygiene compliance and surface cleaning timing on infection risk reductions with a mathematical modeling approach, American Journal of Infection Control, 47 (2019) 1453-1459.

DOI:10.1016/j.ajic.2019.05.023.

[11] A.M. Wilson, M.-F. King, M. López-García, M.H. Weir, J.D. Sexton, R.A. Canales, G.E. Kostov, T.R. Julian, C.J. Noakes, K.A. Reynolds, Evaluating a transfer gradient assumption in a fomite-mediated microbial transmission model using an experimental and Bayesian approach, Journal of the Royal Society Interface, 17 (2020) 20200121. DOI:10.1098/rsif.2020.0121.

[12] S.F. Bloomfield, A.E. Aiello, B. Cookson, C. O'Boyle, E.L. Larson, The effectiveness of hand hygiene procedures in reducing the risks of infections in home and community settings including handwashing and alcohol-based hand sanitizers, American Journal of Infection Control, 35 (2007) S27-S64. DOI:10.1016/j.ajic.2007.07.001.

[13] N. Fierer, M. Hamady, C.L. Lauber, R. Knight, The influence of sex, handedness, and washing on the diversity of hand surface bacteria, Proceedings of the National Academy of Sciences of the United States of America, 105 (2008) 17994-17999. DOI:10.1073/pnas.0807920105.

[14] M. Guo, P. Xu, T. Xiao, R. He, M. Dai, S.L. Miller, Review and comparison of HVAC operation guidelines in different countries during the COVID-19 pandemic, Building and Environment, 187 (2021) 107368. DOI:10.1016/j.buildenv.2020.107368.

[15] S. Kundrapu, V. Sunkesula, L.A. Jury, B.M. Sitzlar, C.J. Donskey, Daily disinfection of high-touch surfaces in isolation rooms to reduce contamination of healthcare workers' hands, Infection Control and Hospital Epidemiology, 33 (2012) 1039-1042. DOI:10.1086/667730.

[16] H. Lei, S. Xiao, B.J. Cowling, Y. Li, Hand hygiene and surface cleaning should be paired for prevention of fomite transmission, Indoor Air, 30 (2020) 49-59. DOI:10.1111/ina.12606.

[17] B. Dybiec, A. Kleczkowski, C.A. Gilligan, Controlling disease spread on networks with

incomplete knowledge, Physical Review. E, Statistical, Nonlinear, and Soft Matter Physics, 70 (2004) 066145. DOI:10.1103/PhysRevE.70.066145.

[18] K. Anderson, S. Lee, C. Menassa, Effect of social network type on building occupant energy use, in: Proceedings of the Fourth ACM Workshop on Embedded Sensing Systems for Energy-Efficiency in Buildings, 2012, pp. 17-24.

[19] H. Lei, Y. Li, S. Xiao, X. Yang, C. Lin, S.L. Norris, D. Wei, Z. Hu, S. Ji, Logistic growth of a surface contamination network and its role in disease spread, Scientific Reports, 7 (2017) 14826. DOI:10.1038/s41598-017-13840-z.

[20] P. Wang, N. Zhang, T. Miao, J.P.T. Chan, H. Huang, P.K.H. Lee, Y. Li, Surface touch network structure determines bacterial contamination spread on surfaces and occupant exposure, Journal of Hazardous Materials, 416 (2021) 126137. DOI:10.1016/j.jhazmat.2021.126137.

[21] N. Zhang, Y. Li, H. Huang, Surface touch and its network growth in a graduate student office, Indoor Air, 28 (2018) 963-972. DOI:10.1111/ina.12505.

[22] S. Xiao, R.M. Jones, P. Zhao, Y. Li, The dynamic fomite transmission of Methicillin-resistant *Staphylococcus aureus* in hospitals and the possible improved intervention methods, Building and Environment, 161 (2019) 106246. DOI:10.1016/j.buildenv.2019.106246.

[23] X. Liu, Z. Peng, X. Liu, R. Zhou, Dispersion characteristics of hazardous gas and exposure risk assessment in a multiroom building environment, International Journal of Environmental Research and Public Health, 17 (2019). DOI:10.3390/ijerph17010199.

[24] M.D.F. Shirley, S.P. Rushton, The impacts of network topology on disease spread, Ecological Complexity, 2 (2005) 287-299. DOI:10.1016/j.ecocom.2005.04.005.

[25] P. Kumar, A. Sinha, Information diffusion modeling and analysis for socially interacting networks, Social Network Analysis and Mining, 11 (2021) 11. DOI:10.1007/s13278-020-

00719-7.

[26] N. Masuda, P. Holme, Temporal network epidemiology, Springer, 2017.

[27] P. Zhao, Y. Li, Modeling and experimental validation of microbial transfer via surface touch, Environmental Science & Technology, 55 (2021) 4148–4161. DOI:10.1021/acs.est.0c04678.

[28] P. Zhao, Y. Li, T.-L. Tsang, P.-T. Chan, Equilibrium of particle distribution on surfaces due to touch, Building and Environment, 143 (2018) 461-472. DOI:10.1016/j.buildenv.2018.07.023.

[29] C.E. Shannon, A mathematical theory of communication, Bell System Technical Journal, 27 (1948) 379-423. DOI:10.1002/j.1538-7305.1948.tb01338.x.

[30] A.-L. Barabási, R. Albert, Emergence of scaling in random networks, Science, 286 (1999) 509-512. DOI:10.1126/science.286.5439.509.

[31] P. Erdos, A. Rényi, On the evolution of random graphs, Publ. Math. Inst. Hung. Acad. Sci, 5 (1960) 17-60.

[32] Q. Wang, Y. Li, D.C. Lung, P.T. Chan, C.H. Dung, W. Jia, T. Miao, J. Huang, W. Chen, Z. Wang, K.M. Leung, Z. Lin, D. Wong, H. Tse, S.C.Y. Wong, G.K. Choi, J.Y. Lam, K.K. To, V.C. Cheng, K.Y. Yuen, Aerosol transmission of SARS-CoV-2 due to the chimney effect in two high-rise housing drainage stacks, Journal of Hazardous Materials, 421 (2021) 126799. DOI:10.1016/j.jhazmat.2021.126799.

[33] WHO, WHO guidelines on hand hygiene in health care: a summary, in: First global patient safety challenge, World Health Organization, Geneva, Switzerland, 2009.

[34] B.M. Dzidek, M.J. Adams, J.W. Andrews, Z. Zhang, S.A. Johnson, Contact mechanics of the human finger pad under compressive loads, Journal of The Royal Society Interface, 14 (2017) 20160935. DOI:10.1098/rsif.2016.0935.

[35] W. Whyte, W. Carson, A. Hambraeus, Methods for calculating the efficiency of bacterial

surface sampling techniques, Journal of Hospital Infection, 13 (1989) 33-41. DOI:10.1016/0195-6701(89)90093-5.

[36] P. Zhao, Y. Li, New sequential-touch method to determine bacterial contact transfer rate from finger to surface, Journal of Applied Microbiology, 127 (2019) 605-615. DOI:10.1111/jam.14332.

[37] F. Escolano, E.R. Hancock, M.A. Lozano, Heat diffusion: Thermodynamic depth complexity of networks, Physical Review E, 85 (2012) 036206. DOI:10.1103/PhysRevE.85.036206.

[38] V. Nicosia, F. Bagnoli, V. Latora, Impact of network structure on a model of diffusion and competitive interaction, EPL (Europhysics Letters), 94 (2011) 68009. DOI:10.1209/0295-5075/94/68009.

[39] M. Lin, N. Li, Scale-free network provides an optimal pattern for knowledge transfer, Physica A: Statistical Mechanics and its Applications, 389 (2010) 473-480. DOI:10.1016/j.physa.2009.10.004.

[40] J. Moody, Network Structure and Diffusion, Duke Population Research Institute Online Working Papers Series, (2009).

[41] J.-C. Delvenne, R. Lambiotte, L.E. Rocha, Diffusion on networked systems is a question of time or structure, Nature Communications, 6 (2015) 1-10. DOI:10.1038/ncomms8366.

[42] P. Holme, Temporal network structures controlling disease spreading, Physical Review E, 94 (2016). DOI:10.1103/PhysRevE.94.022305.

[43] J.M. Read, K.T. Eames, W.J. Edmunds, Dynamic social networks and the implications for the spread of infectious disease, Journal of The Royal Society Interface, 5 (2008) 1001-1007. DOI:10.1098/rsif.2008.0013.

[44] M.F. Shlesinger, B.J. West, Complex fractal dimension of the bronchial tree, Physical Review Letters, 67 (1991) 2106-2108. DOI:10.1103/PhysRevLett.67.2106.

[45] L.K. Uahabi, M. Atounti, New approach to the calculation of fractal dimension of the lungs, Annals of the University of Craiova-Mathematics and Computer Science Series, 44 (2017) 78-86.

[46] G. Werner, Fractals in the nervous system: conceptual implications for theoretical neuroscience, Frontiers in Physiology, 1 (2010) 00015. DOI:10.3389/fphys.2010.00015.

[47] O.M. Bruno, R. de Oliveira Plotze, M. Falvo, M. de Castro, Fractal dimension applied to plant identification, Information Sciences, 178 (2008) 2722-2733. DOI:10.1016/j.ins.2008.01.023.

[48] H. Lei, Y. Li, S. Xiao, C.H. Lin, S.L. Norris, D. Wei, Z. Hu, S. Ji, Routes of transmission of influenza A H1N1, SARS CoV, and norovirus in air cabin: comparative analyses, Indoor Air, 28 (2018) 394-403. DOI:10.1111/ina.12445.

[49] S. Xiao, Y. Li, M. Sung, J. Wei, Z. Yang, A study of the probable transmission routes of MERS-CoV during the first hospital outbreak in the Republic of Korea, Indoor Air, 28 (2018) 51-63. DOI:10.1111/ina.12430.

[50] Y. Xiao, Y. Zhou, S. Tang, Modelling disease spread in dispersal networks at two levels, Mathematical Medicine and Biology : a Journal of The IMA, 28 (2011) 227-244. DOI:10.1093/imammb/dqq007.

[51] Q. Wang, C. Zhang, C. Ren, J. Hang, Y. Li, Urban heat island circulations over the Beijing-Tianjin region under calm and fair conditions, Building and Environment, 180 (2020) 107063. DOI:10.1016/j.buildenv.2020.107063.

[52] A.B. Hansen, C.S. Witham, W.M. Chong, E. Kendall, B.N. Chew, C. Gan, M.C. Hort, S.-Y. Lee, Haze in Singapore–source attribution of biomass burning PM 10 from Southeast Asia, Atmospheric Chemistry and Physics, 19 (2019) 5363-5385. DOI:10.5194/acp-19-5363-2019.

[53] Z. Wei, L. Wang, S. Ma, F. Zhang, J. Yang, Source contributions of PM2. 5 in the severe

haze episode in Hebei cities, The Scientific World Journal, 2015 (2015). DOI:10.1155/2015/480542.

[54] S. Xiao, J.W. Tang, Y. Li, Airborne or fomite transmission for norovirus? A case study revisited, International Journal of Environmental Research and Public Health, 14 (2017) 1571. DOI:10.3390/ijerph14121571.

[55] M.N. Zonouzi, M. Kargari, Modeling uncertainties based on data mining approach in emergency service resource allocation, Computers & Industrial Engineering, 145 (2020) 106485. DOI:10.1016/j.cie.2020.106485.

[56] W. Chen, G. Zhai, C. Ren, Y. Shi, J. Zhang, Urban resources selection and allocation for emergency shelters: In a multi-hazard environment, International Journal of Environmental Research and Public Health, 15 (2018) 1261. DOI:10.3390/ijerph15061261.

[57] P. Davidsson, L. Henesey, L. Ramstedt, J. Törnquist, F. Wernstedt, An analysis of agent-based approaches to transport logistics, Transportation Research part C: emerging technologies, 13 (2005) 255-271. DOI:10.1016/j.trc.2005.07.002.

[58] O. Woolley-Meza, C. Thiemann, D. Grady, J.J. Lee, H. Seebens, B. Blasius, D. Brockmann, Complexity in human transportation networks: a comparative analysis of worldwide air transportation and global cargo-ship movements, The European Physical Journal B, 84 (2011) 589-600. DOI:10.1140/epjb/e2011-20208-9.

[59] N. Shinohara, J. Sakaguchi, H. Kim, N. Kagi, K. Tatsu, H. Mano, Y. Iwasaki, W. Naito, Survey of air exchange rates and evaluation of airborne infection risk of COVID-19 on commuter trains, Environment International, 157 (2021) 106774. DOI:10.1016/j.envint.2021.106774.

[60] S. Karimzadeh, R. Bhopal, H.N. Tien, Review of infective dose, routes of transmission and outcome of COVID-19 caused by the SARS-COV-2: comparison with other

respiratory viruses, Epidemiology & Infection, 149 (2021). DOI:10.1017/S0950268821000790.

Figure 1. Graphical representations of 10 networks: (a) networks I–V, which have four nodes; (b) network VI, which has eight nodes; (c) networks VII–X, which have five nodes. In each network, both the nodes and the edges are numbered. In each network, node 1 (gray shadow) is set as the contaminant source and contaminants spread from the source following the edge sequence. The networks with fractal, centralized, and linear structures are denoted with different colors.

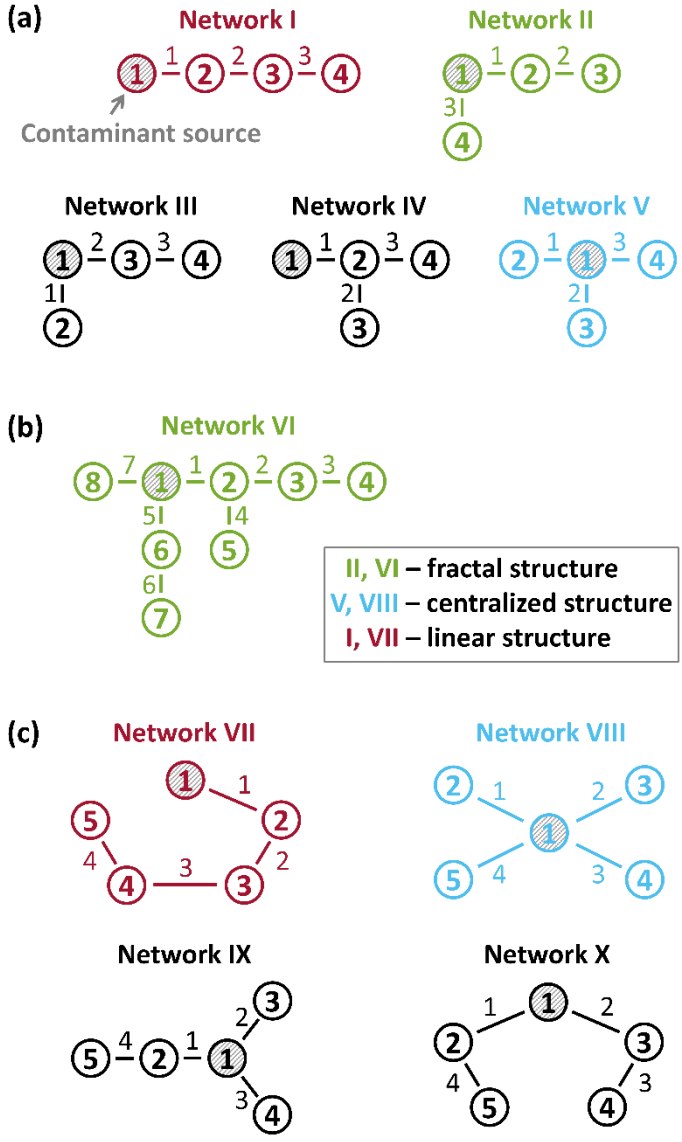

Figure 3 Layout of four multi-compartment cabins designed according to the structures of networks VII–X in Figure 1. Each cabin has five compartments connected by four doors (gray sectors), representing the five nodes and four time-series edges in the corresponding network. In each network, the tracer gas is released in compartment 1 and diffused as the four doors are opened and closed following the edge sequence.

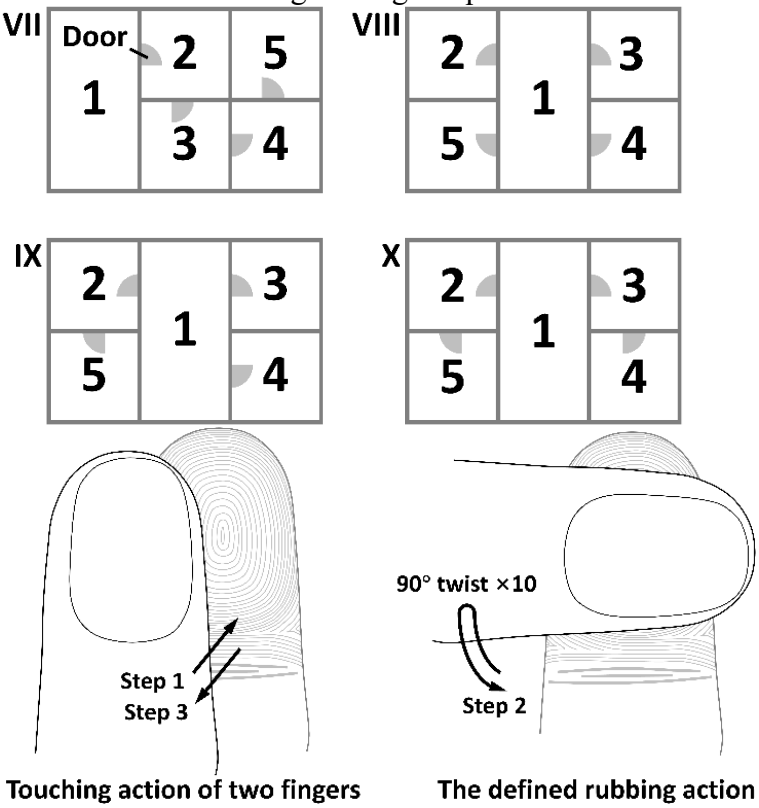

Figure 4 Defined touching patterns. Step 1: the two fingers approach each other. Step 2: the two fingers maintain tight contact for approximately 10 s while performing a twisting 90° back-and-forth movement 10 times. Step 3: the two fingers separate.

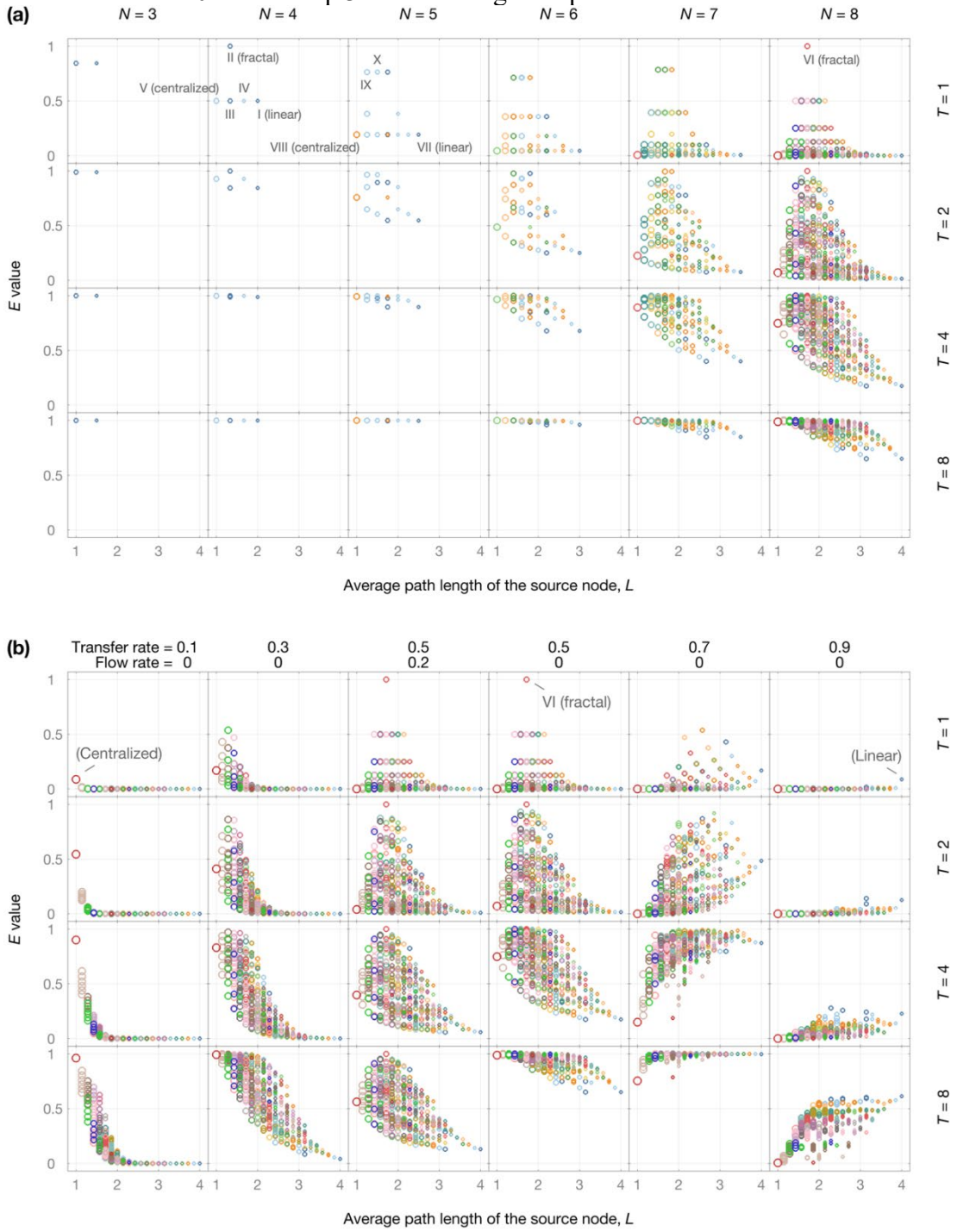

Figure 5 Contaminant distribution evenness in different basic networks ($N \leq 8$) as a function of the average path length of the source node (L). For each network, the evenness after different numbers of interaction rounds (T = 1, 2, 4, and 8) is quantified by the newly defined parameter E, which is calculated under (a) different numbers of nodes (N) with a constant transfer rate (τ = 0.5) and flow rate (R_{Flow} = 0); (b) different transfer rates (τ) and flow rates (R_{Flow}) with a constant number of nodes (N = 8). Each circle in a plot represents a network and is characterized by the degree of the source node (D, proportional to the symbol area) and the network framework (distinguished by the symbol color). The circles denoted by Roman numerals correspond to the networks in Figure 1.

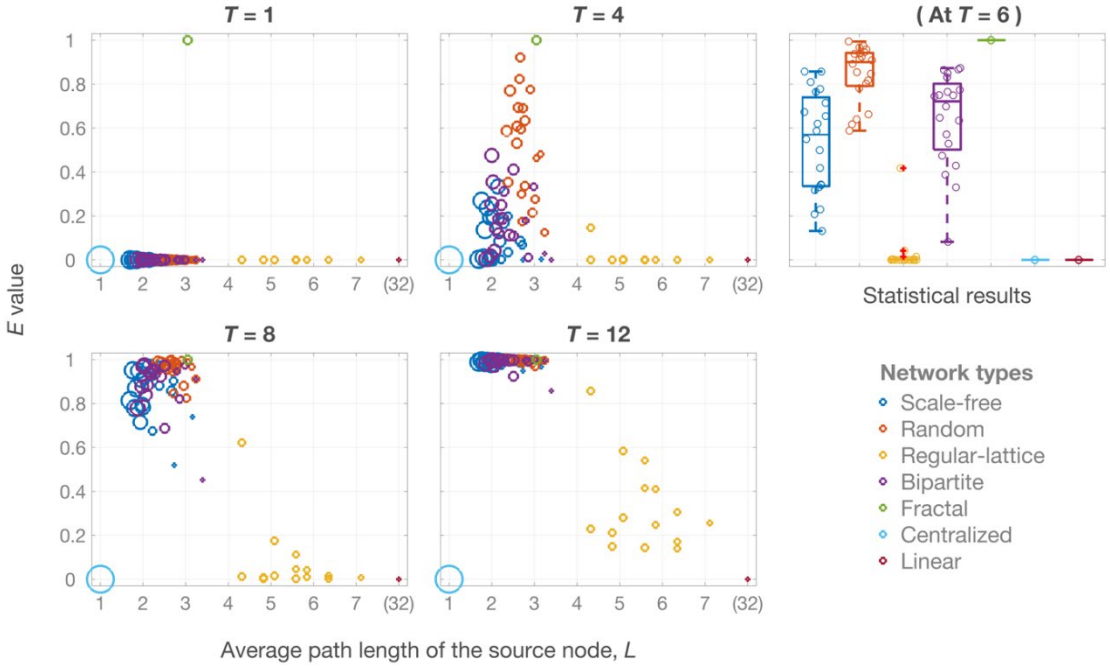

Figure 6 Contaminant distribution evenness in different complex networks (N = 64) as a function of the average path length of the source node (L). For each network, the evenness after different numbers of interaction rounds (T = 1, 4, 8, and 12) is quantified by the newly defined parameter E, which is calculated with a transfer rate of τ = 0.5. Each circle in a plot represents a network and is characterized by the degree of the source node (D, proportional to the symbol area) and the network category (distinguished by the symbol color). A statistical result of the E values at T = 6 is presented to illustrate the average and various values of contaminant spreading efficiency for each network type.

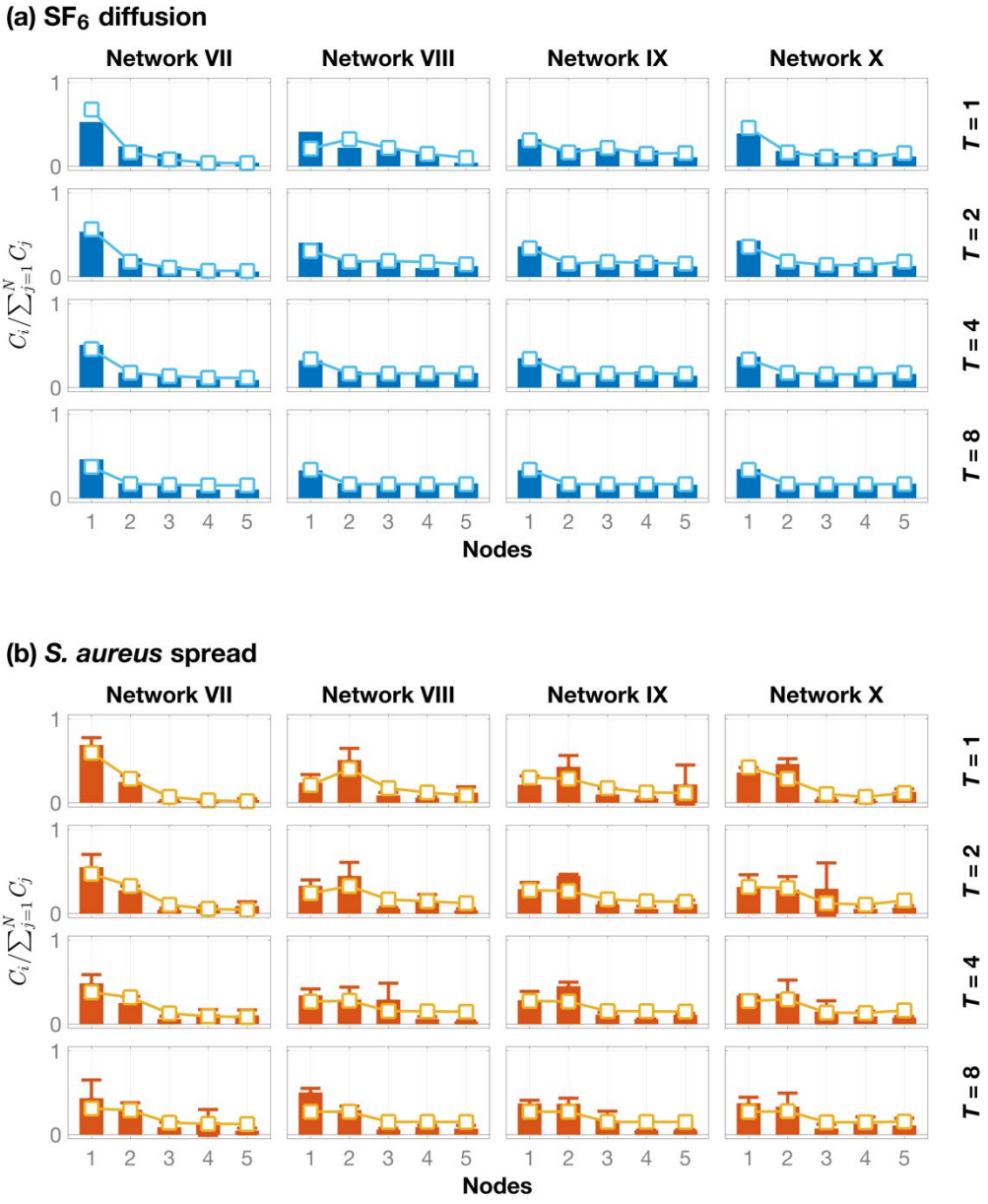

Figure 7 Experimental data (columns) and theoretical predicted results (square symbols) of contaminant spreading in four networks (networks VII–X in Figure 1). In each network, the contaminant proportion on each node ($C_i / \sum_{j=1}^{N} C_j$) varies with increasing interaction round (T). (a) SF_6 diffusion in multi-compartment cabins; (b) *S. aureus* spread in multi-finger networks, in which the error bars represent the standard deviations of three replicates in experiments.

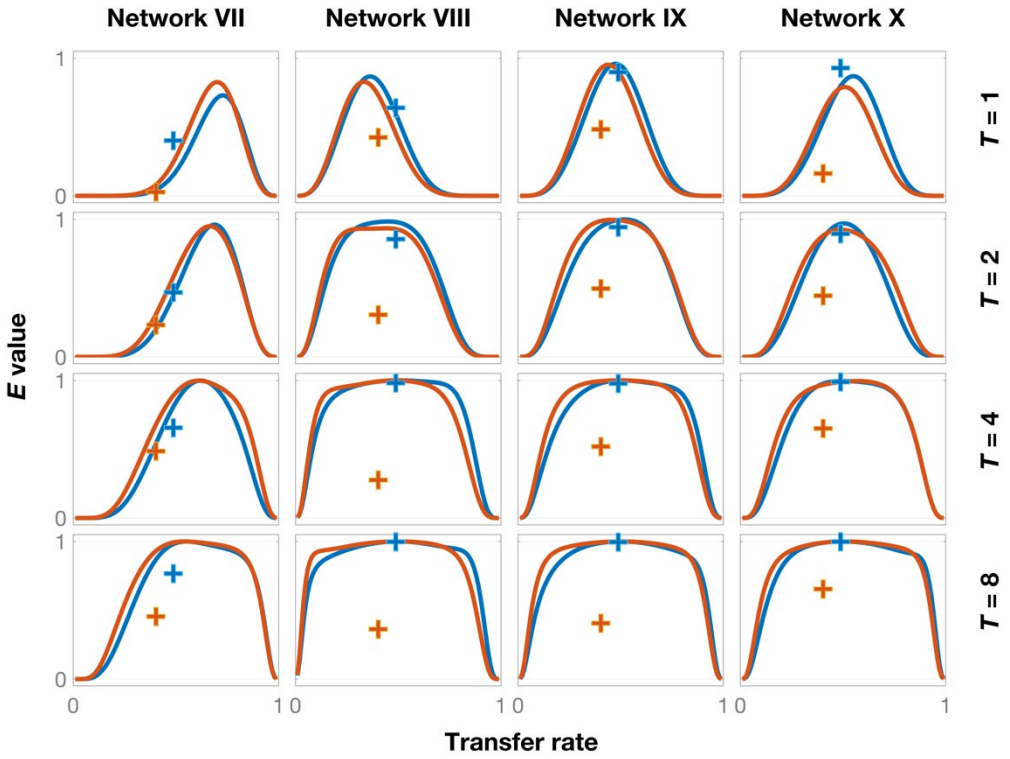

Figure 8 Comparison of the E values based on the predicted results and experimental data from Figure 6 (blue: SF_6 diffusion; red: *S. aureus* spread). For each network (VII–X in Figure 1) and interaction round (T = 1, 2, 4, or 8), a series of predicted E values (curve) was derived with a transfer rate of τ = 0–1; the experimental E value (cross point) was obtained according to the experimental data in the corresponding plot in Figure 6. We measured the transfer rate from a separate experiment (τ = 0.488 in SF_6 diffusion; τ = 0.403 in *S. aureus* spread) to determine the horizontal positions of the cross-points.

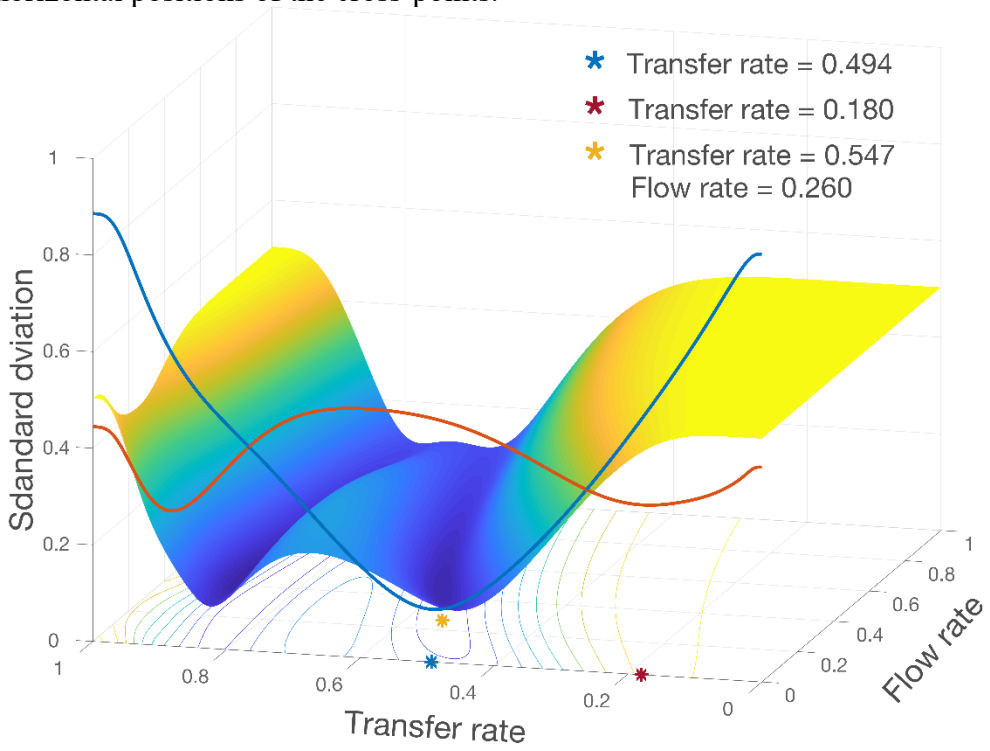

Table 1 Assignment of fingers to the nodes in each designed network. The structures of networks VII–X are shown in Figure 1. In each network, node 1 is the bacteria source.

Networks	**Node 1**	**Node 2**	**Node 3**	**Node 4**	**Node 5**	***L***	***D***
VII	Left thumb	Right thumb	Left index	Right index	Left middle	2.5	1
VIII	Left thumb	Right thumb	Right index	Right middle	Right ring	1	4
IX	Left thumb	Right thumb	Right index	Right middle	Left index	1.2	3
X	Left thumb	Right thumb	Right index	Right middle	Left index	1.5	2

2.2.5 Estimation of per-interaction transfer rate based on E values

Table 2 Effects of different parameters on contaminant spreading efficiency represented by the *E* value.

Parameters	**Effect on *E* value** [a]	
	$\tau \to 0$	$\tau \to 1$
Interaction round, *T*	+	+
Number of edges, *M* (∝ average degree in a network) (∝ network density)	+	+
Degree of source node, *D* (∝ degree centrality of source node)	+	−
Average path length of source node, *L*	−	+
Average path length in a network	−	+
Network diameter	−	+
Number of nodes, *N*	−	−
Contaminant flow, R_{Flow}	−	−
Contaminant decay, R_{Decay}	NE	NE

[a] + (−) represents a positive (negative) effect, indicating that the *E* value increased (decreased) with an increase in the value of the parameter; and NE represents that the parameter has no effect on the *E* value.